Hindawi
International Journal of Photoenergy
Volume 2022, Article ID 6094360, 8 pages
https://doi.org/10.1155/2022/6094360

Research Article

Study on Lubrication-Photothermal Synergistic Deicing of CNT Coating on Wind Turbine Blades

Jianjun He,[1] Huanyu Tian,[1] Kaijun Yang,[1] Jun Jie,[2] Biao Chen,[2] Zhonghu Shu,[2] Jiangyong Bao,[1] and Min Pu[1]

[1]*School of Energy and Power Engineering, Changsha University of Science and Technology, Changsha 410114, China*
[2]*Longyuan Jiangyong Wind Power Generation Co., Ltd. of CHN Energy Group, Changsha 410000, China*

Correspondence should be addressed to Kaijun Yang; ykj765240712@163.com

Received 19 August 2021; Revised 17 December 2021; Accepted 11 February 2022; Published 11 March 2022

Academic Editor: Dillip K. Panda

Aiming at the problem of wind turbine blades' icing, a carbon nanotube composite photothermal coating with both active deicing and passive anti-icing properties was prepared by the spin-coating method. The results indicate that the lubricating coating doped with carbon nanotubes can effectively delay freezing time and reduce ice adhesion strength. The spin-coated 6-layer coating can achieve the best photothermal conversion performance and consume relatively few nanomaterials to maximize the capture of energy in near-infrared light. Under the irradiation of near-infrared light (808 nm), the surface temperature of the coating can reach 97.1°C, which has good photothermal conversion performance. The antifrosting ability of carbon nanotube nanocomposite photothermal coating is related to the content of lubricating oil, and the defrosting performance is related to the content of carbon nanotubes in the coating. Adopting the lubrication-photothermal synergistic deicing method can greatly shorten the deicing time, which is compared with only using photothermal deicing from 392 s to 51 s.

1. Introduction

The icing of wind turbine blades is one of the important factors affecting power generation efficiency of wind turbines [1, 2]. Traditional solutions to the problem of blade icing include solution deicing [3], mechanical deicing [4], thermal deicing [5], and pneumatic deicing [6]. These deicing methods are difficult to operate and require external force, with low efficiency and high energy consumption. They generally play an auxiliary role and do not have broad development space. Coating anti-icing is an ideal anti-icing method with low energy consumption and no pollution [7], which generally include superhydrophobic coating [8], self-lubricating coating [9], and photothermal coating [10].

In recent years, superhydrophobic surfaces have been widely used in the field of anti-icing due to their ability to reduce ice adhesion strength and delay icing [11–14].

The contact between ice and hydrophilic surface belongs to the traditional solid-solid contact model, while the contact between ice and superhydrophobic surface belongs to the solid-gas-solid contact model. The superhydrophobic surface is obtained through low surface energy modification and micronanorough structure construction. The air filled in the micronanorough structure acts as an "air cushion" thermal insulation layer to achieve "air film isolation", thereby delaying icing [15]. However, under high humidity conditions, the superhydrophobic surface will have the problem of anti-icing failure [16]. The Aizenberg research group of Harvard University first prepared a smooth liquid injection porous surface (SLIPS) with lubricating properties. It has a slight sliding angle, low contact angle hysteresis, and self-healing characteristics when damaged [17]. On this basis, Subramanyam et al. [18] found that a surface containing lubricating fluid would reduce the adhesion of ice by 75%. The principle [19] is that the increase of Laplace pressure makes the closely arranged columns that have excellent lubricant retention ability, so that the closely arranged columns maintain a smoother substrate/ice interface. Compared with the

air filled in the gap of the rough structure of the superhydrophobic surface, the lubricating oil filled in the gap of the rough structure of the supersmooth surface has strong self-healing ability and pressure stability [20]. Kim et al. [21] found that in a frosted environment, more than 90% of the surface of the layered superhydrophobic coating was covered by frost within 80 minutes, while the coverage rate of the supersmooth liquid-soaked surface was less than 20%. Smooth liquid injection porous surface has been proved to be the most effective method to reduce the strength of ice adhesion and prolong the freezing time [22]. Both the superhydrophobic coating and the self-lubricating coating only have a passive anti-icing effect and can still be covered by ice at extremely low temperatures.

Current research has found that there are many materials that exhibit photothermal effects, which can be caused by thermal energy generated by photon radiation. These materials can absorb radiation in a large frequency range and convert it into thermal energy [23, 24], which can be used in the coating to achieve the effect of active deicing. Yin et al. [25] added Fe_3O_4 particles to the film to melt the ice layer under near-infrared light, demonstrating for the first time the feasibility of using photothermal coating for anti-icing and deicing. Guo et al. [26] prepared a superhydrophobic SiC/CNTs coating with photothermal deicing performance through a simple spraying method, with a contact angle of up to 161°, and a sliding angle as low as 2°, realizing the combination of superhydrophobic anti-icing and near-infrared photothermal deicing.

Carbon nanotubes (CNTs) can quickly heat up under near-infrared radiation [27] and they have high photothermal conversion efficiency. Therefore, CNTs with photothermal properties are introduced as fillers in this paper to explore the effect of the addition of CNTs on the anti-icing and deicing performance of SLIPS coating and to prepare a lubricating-photothermal synergistic deicing CNT coating. It provides a new idea for solving the problem of icing on the surface of wind turbine blades.

2. Materials and Methods

2.1. Materials. Absolute ethanol (AR), n-hexane (AR), liquid paraffin (density 0.84-0.86), Triton X-100 (BC), deionized water (AR), and multiwalled carbon nanotubes (>95%, inner diameter: 5-12 nm, outer diameter: 30-50 nm, length: 10-20 μm) were purchased from Aladdin Corp. Polydimethylsiloxane (PDMS) was purchased from Suzhou Xiaoxi Industrial Products Supermarket Co., Ltd., China.

2.2. Preparation of Samples. The materials required to prepare CNT nanocomposite photothermal coating are shown in Table 1.

The glass sheet with specifications of 20 mm × 20 mm was put into absolute ethanol for ultrasonic cleaning for 1 h to remove oil stains on the surface.11 g of n-hexane, 4 g of liquid paraffin, and 0.04 g of multiwalled CNTs were added to the beaker and stirred evenly with a stirrer. 2.475 g PDMS prepolymer and curing agent were added to the beaker at a ratio of 10 : 1.Then, the mixture in the beaker was ultrasonic dispersed for 0.5 h to obtain a uniform suspension, which was stirred until slightly thick. The stirred mixture was spin-coated on a glass sheet at a rotation speed of 1000 r/min for 30s, as shown in Figure 1. And each layer was placed in a drying oven at 80°C for 5 min. The coatings of 2-layer, 4-layer, 6-layer, 8-layer, and 10-layer were named C-2, C-4, C-6, C-8, and C-10, respectively.

Table 1: The materials of CNT nanocomposite photothermal coating.

Materials	Multiwalled CNTs	Triton X-100	PDMS	n-Hexane	Liquid paraffin
Proportion%	0.2	1.1	14.1	62.1	22.5

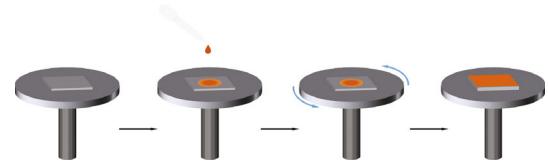

Figure 1: Schematic diagram of spin coating.

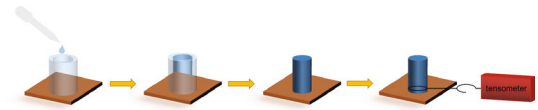

Figure 2: Schematic diagram of ice adhesion strength test device.

2.3. Performance Testing and Characterization. A 200 MAT inverted metallographic microscope was used to characterize the surface morphology of the coating. A device designed by the laboratory was used to test the freezing time of the sample at -20°C and a humidity of 80%. The freezing time is defined as the duration of the droplet condensation process from the liquid phase to the solid phase until the droplet completely turns into ice. Use the laboratory self-designed device in Figure 2 to test the ice adhesion strength after freezing, and the ice adhesion strength is defined as the pulling force required for the ice shedding surface divided by the contact area between the ice and the coating. Use a near-infrared light emitter with a wavelength of 808 nm and a power of 1w to test the photothermal performance of the sample and record the time it takes to melt the ice on the surface of the sample in the icing test platform. Use the icing test platform for the antifrost and defrost tests. To perform the photothermal-lubrication synergistic deicing experiment, set the surface of the icing test platform at an inclination angle of 30°, 60°, and 90°.

3. Results and Discussion

3.1. Anti-Icing Performance of CNT Nanocomposite Photothermal Coating

3.1.1. Freezing Time of Supercooled Water. Set the temperature of the icing experiment platform to -20°C and humidity of 80% and conduct supercooled water icing tests on different thickness coating. Freezing time on the surface of CNT nanocomposite photothermal coating is shown in Figure 3. The icing time increases as the thickness of the coating

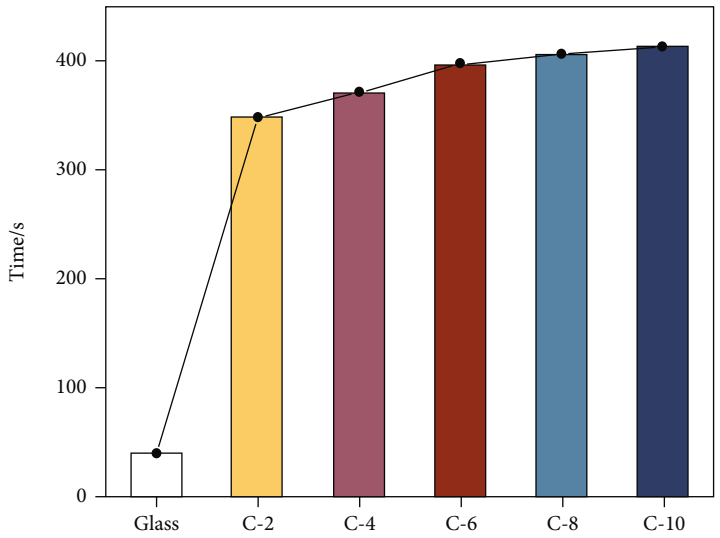

Figure 3: Freezing time on the surface of CNT nanocomposite photothermal coating.

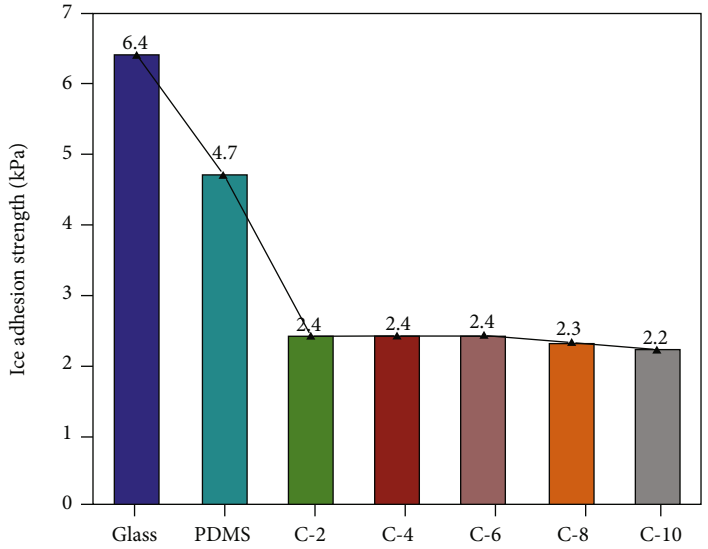

Figure 4: The test results of ice adhesion strength.

increases. Compared with untreated glass sheet, the freezing time on the surface of C-10 is extended to 413 s. It shows that the rough structure of CNTs on the surface has good delayed icing performance. Because the diameter of CNTs is on the nanometer scale and the length is on the micrometer scale, the micronanocomposite structure is formed in the process of constructing the surface, which can reduce the contact area between the water droplet and the surface during the crystallization process [28]. Such a structure is similar to the hydrophobic mechanism of a superhydrophobic coating. At the same time, the lubricating oil between the ice layer and surface can also reduce the heat exchange with the outside world to achieve delayed icing.

3.1.2. Ice Adhesion Strength Test. The test results of ice adhesion strength are given in Figure 4. It can be seen that the ice adhesion strength of coating with different layers are close. The reason is that pdms and CNTs are the main factors that affect the strength of ice adhesion, while all coatings use PDMS as the substrate, and the spin coating method contains a similar number of CNTs in each layer. The ice adhesion strength drops from 2.4 kPa of C-2 to 2.2 kPa of C-10, and the surface ice adhesion strength of C-10 is only 35.1% of the glass surface, which is greatly reduced compared with the glass substrate and PDMS substrate. On the one hand, as coating thickness increases, ice adhesion strength decreases, and the lubricant on the surface is blocked between the ice layer and coating. The interfacial slip provided by the miscible chain improves the elastomer network and effectively reduces the ice adhesion strength. On the other hand, the main component of the coating, PDMS, is an elastomer [29], which has properties similar to solids and liquids. The crosslinking density and physical stiffness exhibited can reduce the shear force and achieve the effect of reducing ice adhesion strength.

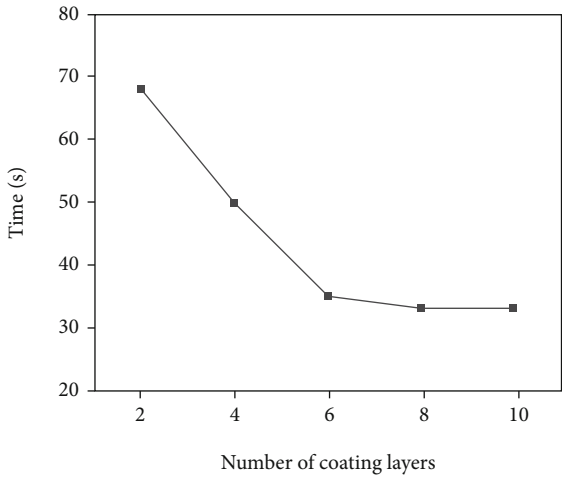

Figure 5: The change of deicing time with the number of coating layers.

3.2. Photothermal Performance of CNT Nanocomposite Photothermal Coating

3.2.1. Photothermal Deicing Performance. The photothermal deicing performance test of the CNT nanocomposite photothermal coating is carried out. The results show that glass and PDMS without CNTs do not have deicing performance. Figure 5 shows the change of deicing time with the number of coating layers. It only takes 68 s for ice to melt on the surface of C-2, indicating that CNT nanocomposite photothermal coating has a good photothermal effect. Both PDMS and CNT nanoparticles have good thermal conductivity, heat can be effectively transferred in the coating, and the ice on the surface of the coating can be quickly melted. As the coating thickness increases, the deicing time decreases. Compared with C-2, the ice melting time of C-6 has been shortened by half, and the photothermal performance has been greatly improved. The melting time of C-6, C-8, and C-10 are similar. It shows that after C-6, its photothermal conversion performance has not increased due to the increase in thickness, and the CNT particles that can generate local surface plasmon resonance are saturated. The increase in thickness wastes raw materials, and the performance improvement is not obvious. Therefore, the photothermal performance of the coating is optimized at this time.

3.2.2. Thermal Infrared Imaging Analysis. Considering economy and photothermal performance, use the C-6 with the best overall performance for thermal infrared imaging analysis, use a thermal infrared imager to observe the surface of the coating irradiated by near-infrared light, and take a picture every 12 s. As shown in Figure 6, it can be seen from the thermal infrared imaging that the surface temperature of the coating has increased significantly. The temperature of CNT nanocomposite photothermal coating increased to 99.1°C in only 20s. And after 60s, the surface temperature of the coating increased to 122.1°C, and then the temperature no longer increased, indicating that the photothermal conversion of CNT nanocomposite photothermal coating has reached equilibrium within 60 s. During the entire heating process,

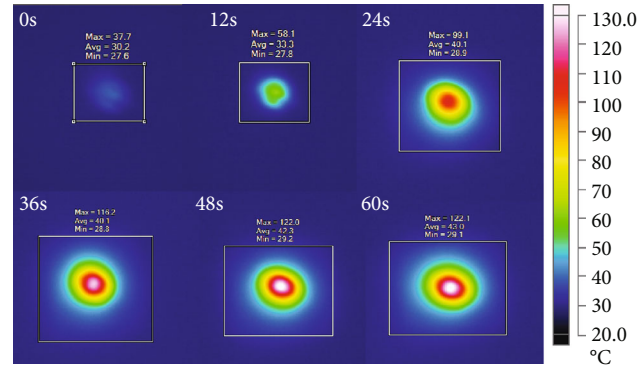

Figure 6: Thermal infrared imaging of C-6 surface.

the first 24 s of photothermal conversion efficiency is the highest, indicating that CNTs have better photothermal conversion performance.

It can be seen from the temperature distribution at six different time points in the thermal infrared image that the temperature at the center point is the highest, and the temperature spreads from the center point to the surroundings. And in the process of diffusion, the temperature keeps decreasing until it is the same as the ambient temperature. This central point is the point where the near-infrared light is irradiated on the coating. At the irradiated point, the CNT nanoparticles in the coating have a local surface plasmon resonance (LSPR) [30]. When the incident electromagnetic (EM) frequency matches the natural frequency of the oscillating surface electron, the local surface plasmon resonance is driven by photon or electron excitation to generate a local electric field. The electrons accelerated through this field can absorb enough energy to exceed the equilibrium configuration and effectively switch the local electric field, thus causing the oscillation. This oscillation is not permanent and requires electromagnetic excitation for maintenance; so, the coating needs to be continuously irradiated with near-infrared light to generate enough energy to heat up. As shown in Formula (1), the frequency of oscillation ω_p is determined by local electron density N, electron charge e, electron mass m, and free space dielectric constant $\mathscr{E}_0$.

$$\omega_p = \sqrt{Ne^2/m\mathscr{E}_0}. \quad (1)$$

When CNTs produce LSPR, heating becomes very efficient. This heat continuously diffuses outwards on the surface, forming a circular temperature gradient distribution. The minimum temperature change on the coating is small, indicating that the heat is only transferred on the surface of the coating and not diffused into the external environment.

3.2.3. Antifrost/Defrost Performance. To simulate the photothermal performance of the photothermal deicing lubricating coating in the real natural environment, an antifrost test was carried out on the icing test platform. The results show that the surface of the glass sheet and the surface of the PDMS have all been frosted. Figure 7 shows the frosting on the coating surface of C-2, C-4, and C-6 after being

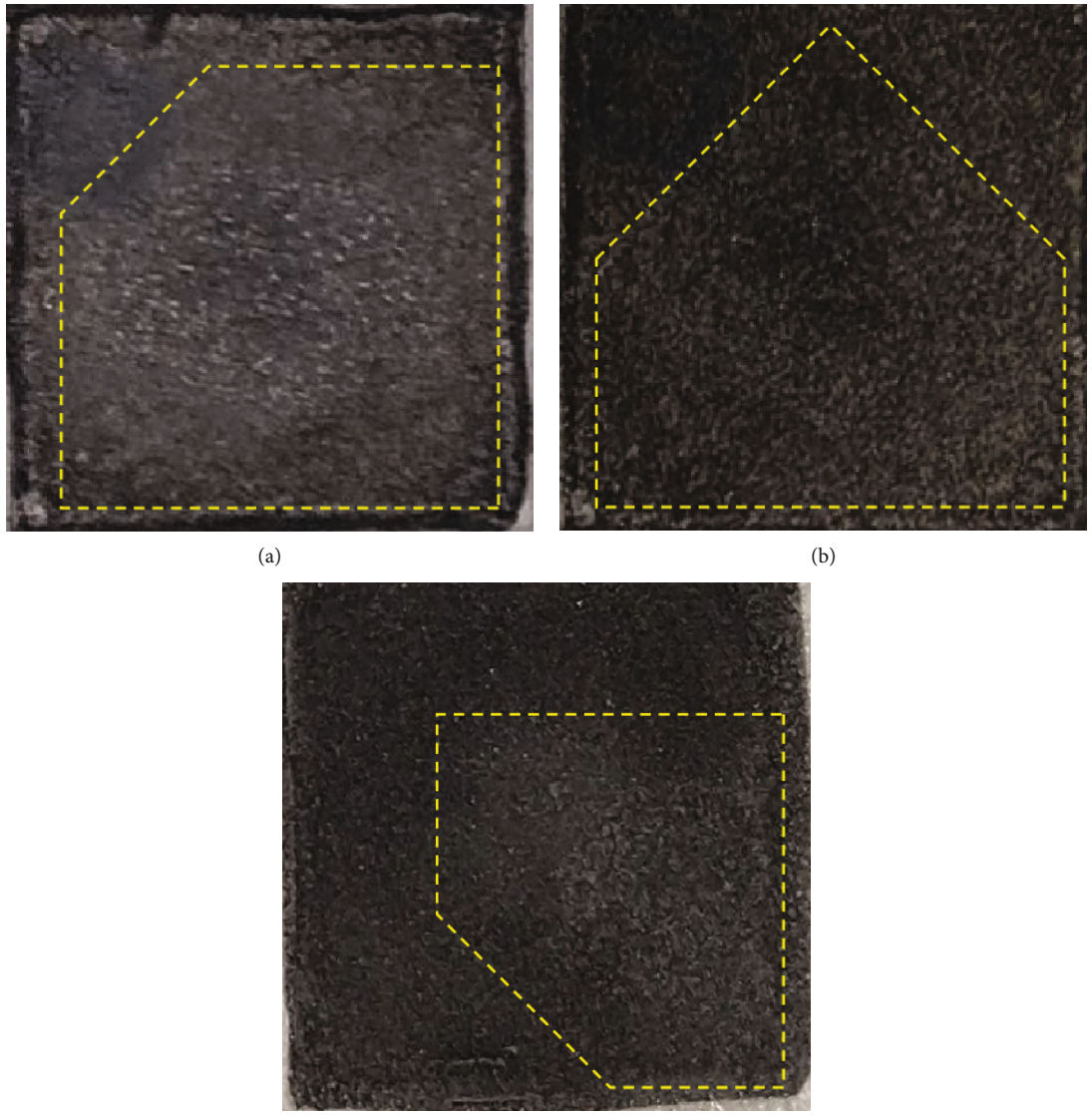

Figure 7: Frost on different surfaces. (a) C-2. (b) C-4. (c) C-6.

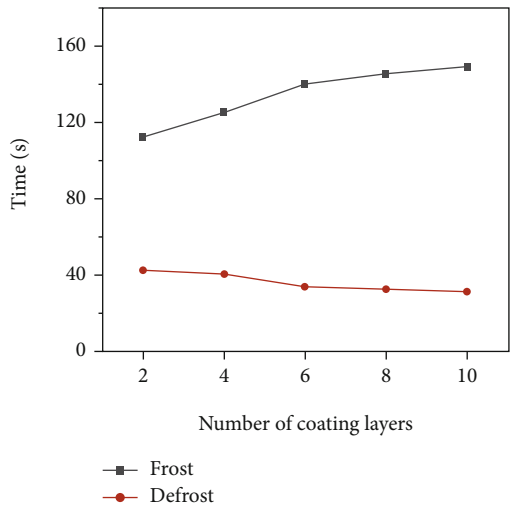

Figure 8: Frost/defrost time of different coating.

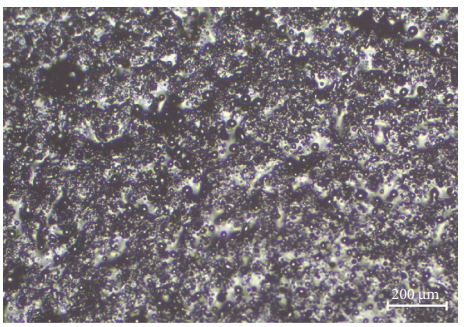

Figure 9: Metallographic diagram of CNT nanocomposite photothermal coating.

placed on an icing test bench for two hours at the same time. It can be seen that the surface of C-2 has been frosted on a large scale, and C-4 and C-6 are also partially frosted. The frosted area on the surface of C-6 is slightly smaller than that

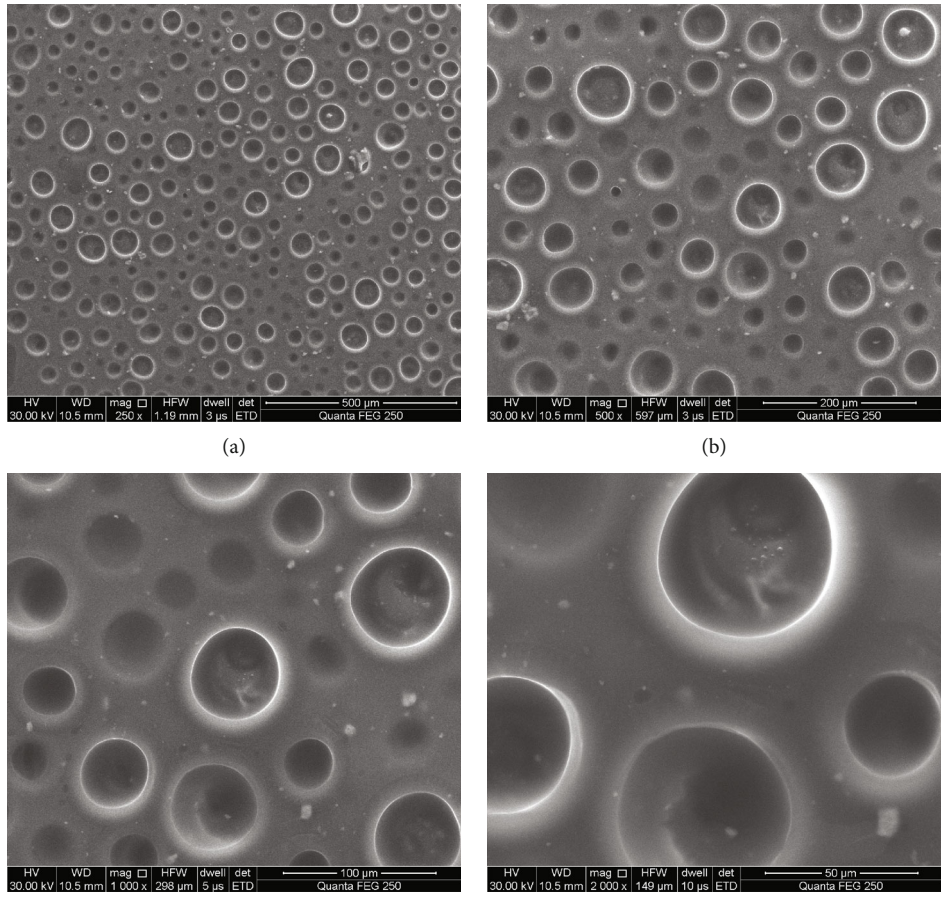

Figure 10: SEM images of CNT nanocomposite photothermal coating with different magnifications. (a) 2000. (b) 1000. (c) 500. (d) 250.

of C-4. Since the freezing point of the lubricant on the coating surface is very low, it still exists in a liquid form at -20°C, blocking the air and the coating surface, reducing the heat transfer on the coating surface, in order to achieve the effect of inhibiting frosting. The lubricating oil on the coating surface plays a key role in inhibiting frosting. And the more layers, the more lubricating oil in the coating.

After the frosting process is over, the surface defrosting experiment is carried out with a near-infrared light emitter. Since the glass sheet and PDMS do not have photothermal properties, the ice on the surface does not melt under the irradiation of near-infrared light. The defrosting time of coating is shown in Figure 8. The surface of C-6 completely melted the frost on the coating surface in only 34 s, and the defrosting process of C-2 also took only 42 s. Due to the excellent thermal conductivity of the PDMS substrate and the CNTs as the carbon-based material itself has good thermal conductivity, the heat generated by the local surface plasma oscillation can be quickly transferred to the surface, and the frosting process is only a thin layer of frost on the coating surface, which can be quickly defrosted under the influence of high temperature.

3.3. Microscopic Morphology Analysis of CNT Nanocomposite Photothermal Coating. Considering economy and photothermal performance, use the C-6 with the best overall performance for metallographic and SEM analysis. It can be seen from the metallographic diagram of Figure 9 that the entire coating exhibits a neat and uniform distribution, and CNTs are distributed in the colloid, indicating that the spin coating method makes the coating uniformly distributed on the substrate.

Figure 10 indicates the SEM images of CNT nanocomposite photothermal coating with different magnifications. It can be seen that the entire coating is mainly structured with PDMS colloid, and the approximately circular substance in the picture is liquid paraffin, which is distributed in the PDMS colloid in the form of droplets. The size is uniform, some are located in the deep layer, and some are located in the shallow layer, indicating that coating prepared by the spin coating method can wrap a certain amount of liquid paraffin on each layer. When liquid paraffin on the surface of the coating is consumed, the liquid paraffin in the deep layer will be deposited on the surface, so that the coating has always been lubricated.

3.4. Research on Photothermal-Lubrication Synergistic Deicing. The characteristic of CNT nanocomposite photothermal coating is that it combines nanoparticles with photothermal effect and SLIPS with lubricating properties. Based on the photothermal deicing test, the coating is tilted at a certain angle, so that the ice layer can slide down, which

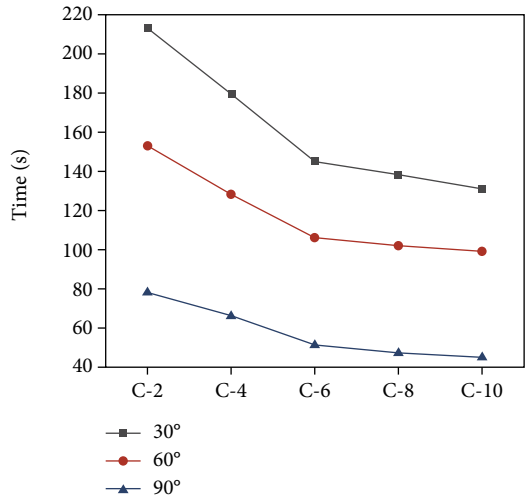

Figure 11: The relationship between ice falling time and the number of coating layers under different inclination angles.

can reflect the advantages of this coating. The results show that the glass sheets and PDMS without CNTs could not cause ice to melt and slip off. Figure 11 shows the time required for different coating with 6 mm ice layer to deicing on inclined surfaces. As the thickness of coating increases, the deicing time continues to decrease, forming an inflection point at the coating C-6. The deicing time of C-6 coating at 30°, 60°, and 90° incline is 145 s, 106 s, and 51 s, respectively. From the results of the photothermal deicing experiment, it is known that the deicing time of surface ice 6 mm placed in the horizontal plane was 392 s. In contrast, the cooperative deicing time is greatly shortened.

Because of the heat generated by near-infrared light on the surface of the coating, the ice at the bottom will melt first. The water generated by melting and the lubricant of the coating itself will reduce the adhesion between ice and coating so that the ice will slide down under the action of gravity. The greater the angle of inclination, the greater the weight of gravity in the plane direction, and the easier it is for ice to slide down. This feature also shows that the photothermal deicing mechanism of the photothermal deicing lubricating coating is not to use near-infrared light to irradiate the ice layer directly to melt ice layer, but to irradiate the surface of the coating through the ice layer and produce heat achieves the effect of deicing.

4. Conclusions

In this paper, a spin-coating method was used to prepare a lubricating-photothermal synergistic deicing CNT coating. The SEM analysis showed that each layer of the coating was covered with a certain amount of liquid paraffin for protection and lubrication. The CNTs did not destroy the anti-icing performance of the layered lubricating coating, but staggered and superimposed in the process of constructing the surface to form a micronanocomposite structure similar to the mechanism of superhydrophobic coating, acting simultaneously with lubricating oil to delay icing time and reduce the strength of ice adhesion. Spin-coated 6-layer coating could consume less nanoparticles and obtain the best photothermal conversion performance. Thermal infrared imaging analysis found that the surface temperature of CNT nanocomposite photothermal coating under the irradiation of near-infrared light rose from 25°C to 122.1°C within 55 s, and the surface ice could be melted within 33 s. The antifrosting ability of CNT nanocomposite photothermal coating is related to the content of lubricating oil, and the defrosting performance is related to the number of CNTs in coating. The CNT nanocomposite photothermal coating adopts lubrication-photothermal synergistic deicing to remove ice on the surface in only 55 s, and the deicing time is shortened by 83% compared with only photothermal deicing. This CNT nanocomposite photothermal coating has good anti-icing and deicing performance, which provides a new idea for engineering applications.

Data Availability

The data used to support the findings of this study are available from the corresponding author upon request.

Conflicts of Interest

The authors declare that they have no conflicts of interest to report regarding the present study.

Acknowledgments

The authors gratefully acknowledge financial support from the National Energy Group Technology Innovation Project (HJLFD).

References

[1] M. Gong, L. Li, R. Liu, P. Zhou, Y. Xiang, and H. Zhang, "Research on ice accretion conditon monitoring reference value and grading diagnosis standard of wind turbine blades," *Acta Energiae Solaris Sinica*, vol. 42, no. 2, pp. 172–178, 2021.

[2] F. Feng, H. Shen, H. Zhao, B. Qu, and Y. Li, "Research on anti-icing characteristics of super-hydrophobic MoSanano-coated blade," *Journal of Engineering Thermophysics*, vol. 42, no. 5, pp. 1168–1175, 2021.

[3] D. Wang, Q. Zhu, Y. Su, J. Li, A. Wang, and Z. Xing, "Preparation of MgAlFe-LDHs as a deicer corrosion inhibitor to reduce corrosion of chloride ions in deicing salts," *Ecotoxicology and Environmental Safety*, vol. 174, pp. 164–174, 2019.

[4] V. Daniliuk, Y. Xu, R. Liu, T. He, and X. Wang, "Ultrasonic deicing of wind turbine blades: performance comparison of perspective transducers," *Renewable Energy*, vol. 145, pp. 2005–2018, 2020.

[5] Y. Wang, A. Ni, J. Wang, H. Hu, and S. Mou, "Experimental study of hybrid de-icing systems combining thermoelectric and hydrophobic coatings," *Fiber Reinforced Plastics/Composites*, vol. 23, no. 8, pp. 68–72, 2016.

[6] K. Wei, Y. Yang, H. Zuo, and D. Zhong, "A review on ice detection technology and ice elimination technology for wind turbine," *Wind Energy*, vol. 23, no. 3, pp. 433–457, 2020.

[7] G. Wang, Y. Shi, L. Jiang, and L. Liu, "Research status of wind turbine blade deicing technology," *Equipment Environmental Engineering*, vol. 13, no. 2, 2016.

[8] J. Bao, J. He, B. Chen et al., "Multi-scale superhydrophobic anti-icing coating for wind turbine blades," *Energy Engineering*, vol. 118, no. 4, pp. 947–959, 2021.

[9] C. Huang and Z. Guo, "Fabrications and applications of slippery liquid-infused porous surfaces inspired from nature: a review," *Journal of Bionic Engineering*, vol. 16, no. 5, pp. 769–793, 2019.

[10] L. Ma, J. Wang, F. Zhao et al., "Plasmon-mediated photothermal and superhydrophobic TiN-PTFE film for anti-icing/deicing applications," *Composites Science and Technology*, vol. 181, p. 107696, 2019.

[11] J. Jiang, G. Lu, and G. Tang, "Inhibition of surface ice nucleation by combination of superhydrophobic coating and alcohol spraying," *International Journal of Heat and Mass Transfer*, vol. 134, pp. 628–633, 2019.

[12] K. R. Murphy, W. T. McClintic, K. C. Lester, C. P. Collier, and J. B. Boreyko, "Dynamic defrosting on scalable superhydrophobic surfaces," *ACS Applied Materials & Interfaces*, vol. 9, no. 28, pp. 24308–24317, 2017.

[13] P. Eberle, M. K. Tiwari, T. Maitra, and D. Poulikakos, "Rational nanostructuring of surfaces for extraordinary icephobicity," *Nanoscale*, vol. 6, no. 9, pp. 4874–4881, 2014.

[14] S. B. Subramanyam, V. Kondrashov, J. Rühe, and K. K. Varanasi, "Low ice adhesion on nano-textured superhydrophobic surfaces under supersaturated conditions," *ACS Applied Materials & Interfaces*, vol. 8, no. 20, pp. 12583–12587, 2016.

[15] Y. Hou, M. Yu, Y. Shang et al., "Suppressing ice nucleation of supercooled condensate with biphilic topography," *Physical review letters*, vol. 120, no. 7, 2018.

[16] S. Jung, M. Dorrestijn, D. Raps, A. Das, C. M. Megaridis, and D. Poulikakos, "Are superhydrophobic surfaces best for icephobicity?," *Langmuir*, vol. 27, no. 6, pp. 3059–3066, 2011.

[17] T. Wong, S. Kang, S. Tang et al., "Bioinspired self-repairing slippery surfaces with pressure-stable omniphobicity," *Nature*, vol. 477, no. 7365, pp. 443–447, 2011.

[18] S. B. Subramanyam, K. Rykaczewski, and K. K. Varanasi, "Ice adhesion on lubricant-impregnated textured surfaces," *Langmuir*, vol. 29, no. 44, pp. 13414–13418, 2013.

[19] X. Su, H. Li, X. Lai et al., "Vacuum-assisted layer-by-layer superhydrophobic carbon nanotube films with electrothermal and photothermal effects for deicing and controllable manipulation," *Journal of Materials Chemistry A*, vol. 6, no. 35, pp. 16910–16919, 2018.

[20] J. Jiang and G. Tang, "Research on the mechanism of anti-icing and ice removal on super-slip surfaces," *Journal of Xi'an Jiaotong University*, vol. 55, no. 8, pp. 111–118, 2021.

[21] P. Kim, T. S. Wong, J. Alvarenga, M. J. Kreder, W. E. Adorno-Martinez, and J. Aizenberg, "Liquid-infused nanostructured surfaces with extreme anti-ice and anti-frost performance," *ACS nano*, vol. 6, no. 8, 2012.

[22] X. Wu and Z. Chen, "A mechanically robust transparent coating for anti-icing and self-cleaning applications," *Journal of Materials Chemistry A*, vol. 6, no. 33, pp. 16043–16052, 2018.

[23] L. Wang, L. Shen, Y. Li, L. Zhu, J. Shen, and L. Wang, "Enhancement of photocatalytic activity on TiO2-nitrogen-doped carbon nanotubes nanocomposites," *International Journal of Photoenergy*, vol. 2013, Article ID 824130, 7 pages, 2013.

[24] J. Conde, J. Rosa, J. C. Lima, and P. V. Baptista, "Nanophotonics for molecular diagnostics and therapy applications," *International Journal of Photoenergy*, vol. 2012, Article ID 619530, 11 pages, 2012.

[25] X. Yin, Y. Zhang, D. Wang et al., "Integration of self-lubrication and near-infrared photothermogenesis for excellent anti-icing/deicing performance," *Advanced Functional Materials*, vol. 25, no. 27, pp. 4237–4245, 2015.

[26] G. Jiang, L. Chen, S. Zhang, and H. Huang, "Superhydrophobic SiC/CNTs coatings with photothermal deicing and passive anti-icing properties," *ACS Applied Materials & Interfaces*, vol. 10, no. 42, pp. 36505–36511, 2018.

[27] X. Li, J. F. Lovell, J. Yoon, and X. Chen, "Clinical development and potential of photothermal and photodynamic therapies for cancer," *Nature Reviews Clinical Oncology*, vol. 17, no. 11, pp. 657–674, 2020.

[28] Q. Liu, Y. Yang, M. Huang, Y. Zhou, Y. Liu, and X. Liang, "Durability of a lubricant-infused electrospray silicon rubber surface as an anti-icing coating," *Applied Surface Science*, vol. 346, pp. 68–76, 2015.

[29] Y. Wang, X. Yao, J. Chen et al., "Organogel as durable anti-icing coatings," *Science China Materials*, vol. 58, no. 7, pp. 559–565, 2015.

[30] P. Ren and X. Yang, "Research progress on surface plasmon resonance of nonmetallic nanomaterials," *Journal of the Chinese Ceramic Society*, vol. 46, no. 10, pp. 1383–1393, 2018.